

Hybrid molecular-continuum fluid dynamics

Rafael Delgado-Buscalioni* and Peter V. Coveney†
*Centre for Computational Science, Department of Chemistry
University College London,
20 Gordon Street, London WC1 OAJ, UK*

We describe recent developments in the hybrid atomistic/continuum modelling of dense fluids. We discuss the general implementation of mass, momentum and energy transfers between a region described by molecular dynamics and the neighbouring domain described by the Navier-Stokes equations for unsteady flow.

PACS numbers:

I. INTRODUCTION

The flow of complex fluids near interfaces is governed by a subtle interplay between the fast microscopic dynamics within a small localised region of the system close to the interface and the slow dynamics in the bulk fluid region. This scenario is encountered in a wide variety of applications ranging from nanotechnology (nanofluidics) and other industrial processes (such as wetting, droplet formation, critical fluids near heated surfaces or crystal growth from a fluid phase) to biological systems (for example, membranes or biomolecules near interfaces). The dynamics of these systems depends on the intimate connection of many different spatio-temporal scales: from the nanoscale to the microscale and beyond. Realistic simulations of such systems via standard classical molecular dynamics (MD) are prohibitive, while continuum fluid dynamics (CFD) cannot describe the important details within the interfacial region. In view of this fact, the field of computer simulation is now faced with the need for new techniques, which bridge a wider range of time and length scales with the minimum loss of information. A hybrid particle-continuum approach provides a resolution to this dilemma. A hybrid algorithm retains all the atomistic detail within the relevant localized domain and couples this region to the continuum hydrodynamic description of the remainder of the system. Indeed hybrid algorithms for liquids can be expected to provide a powerful tool for the fast growing field of nanofluidics in micro electro-mechanical systems (MEMS) and our ongoing contributions have been recognized by the nanoscience community (R. Delgado-Buscalioni and Coveney 2003a) as offering a promising simulation technique with nanotechnological applications.

Hybrid algorithms for solids (Abraham *et al.* 1998) and gases (Garcia *et al.* 1999) were the first to be fully developed in the literature. As expected in most theoretical descriptions of matter, the hybrid description of the liquid state is the most challenging one. The general procedure is to connect the particle domain (P) and the continuum domain (C) within an overlapping region comprised of two buffers: $C \rightarrow P$ and $P \rightarrow C$ (see figure 1). Within the $P \rightarrow C$ buffer the particle dynamics are coarse-grained to extract the boundary conditions for the C-region. The most complicated part of any hybrid scheme is the $C \rightarrow P$ coupling where the microscopic dynamics need to be reconstructed to adhere to the prescriptions given by the continuum variables. Moreover, in doing so the unphysical artifacts thereby introduced should be minimized (following Occam's razor).

In this paper we provide an overview of the state-of-the-art of the hybrid modelling of liquids. In §II we start by presenting an overview of the hybrid scheme and some preliminary topics such as the inherent constraints on the continuum time step and the spatial-grid size. Section III discusses several implementations of the temporal-coupling. The $C \rightarrow P$ coupling scheme is then explained in §IV for the general case of mass, momentum and energy. We illustrate this important part of the scheme by reproducing the three hydrodynamic modes (shear, sound and heat) governing the relaxing flows in an infinite medium. Section V is devoted to the $P \rightarrow C$ coupling, based on a finite volume method solving the flow within the C domain. Some comments on the effect of noise on the accuracy of the scheme are made. The full method is used in §VI to solve the problem of shear flow driven by oscillatory wall motion in a nano-slot. Finally, conclusions and future directions for this research are described in §VII.

*Electronic address: R.Delgado-Buscalioni@ucl.ac.uk

†Electronic address: p.v.coveney@ucl.ac.uk

II. OVERVIEW

The domain decomposition deployed in our hybrid scheme is depicted in figure 1. Within domain P the fluid is described at the atomistic level via Newtonian dynamics. The position of the $N(t)$ atoms at time t inside P is updated each Δt_P time interval using a standard MD scheme. The present calculations were done with a Lennard-Jones (LJ) fluid. Throughout the ongoing discussion all quantities are given in reduced Lennard Jones units: length σ , mass m , energy ϵ , time $(m\sigma^2/\epsilon)^{1/2}$ and temperature ϵ/k_B . We refer to Hoheisel 1996, for the estimated physical values of the LJ parameters for several substances (as an example, for a simple molecular fluid as N₂, $\sigma \simeq 0.35\text{nm}$ and $\epsilon/k_B \simeq 100\text{K}$).

The rest of the computational domain (C) is described by the Navier-Stokes equations. The fluid variables at C are the densities of the conserved quantities for which the equations of motion in conservative form are $\partial\Phi/\partial t = -\nabla \cdot \mathbf{J}_\Phi$ with $\Phi = \{\rho, \rho\mathbf{u}, \rho e\}$ and $\mathbf{J}_\Phi = \{\rho\mathbf{u}, \rho\mathbf{u} + \mathbf{\Pi}, \rho\mathbf{u}e + \mathbf{\Pi} \cdot \mathbf{u} + \mathbf{q}\}$ standing for the mass, momentum and energy fluxes respectively. Here ρ is the density, \mathbf{u} the local velocity, e the specific energy, $\mathbf{\Pi} = P\mathbf{1} + \tau$ the stress tensor which contains the pressure P and the viscous tensor τ (for a Newtonian fluid) and $\mathbf{q} = -\kappa\nabla \cdot T$, the heat flux by conduction expressed via Fourier's law. These continuum equations may be solved via standard CFD methods. Alternatively, for low-Reynolds number flows ($Re \leq O(10)$) the equations can be solved analytically (Delgado-Buscalioni & Coveney 2003b), as is done in the tests presented in §IV.

The kind of information to be transferred in the overlapping region has been the subject of some discussion. The first attempts in the literature (Delgado-Buscalioni & Coveney 2003b and references therein) considered the transfer of momentum in steady shear flows and proposed a matching procedure based on the continuity of velocity across the overlapping region. This sort of coupling strategy may be referred to as “coupling-through-state”. An alternative formulation of the information exchange for liquids based on matching the fluxes of conserved quantities (to/from P and C) was proposed by Flekkøy *et al.* 2000. These authors considered steady shear flows with mass transfer. In subsequent work by Delgado-Buscalioni & Coveney (2003b) the flux-coupling scheme was generalized to enable transfer of mass, energy and momentum (along both transversal and longitudinal directions). Delgado-Buscalioni & Coveney 2003b also present a comparative study of the coupling-through-fluxes and coupling-through-state schemes for flows involving energy transfer (longitudinal waves). It was shown that the coupling-through-fluxes scheme provides the correct physical behaviour, while the coupling-through-state scheme does not guarantee positive entropy production. Consequently the coupling of fluxes is of central importance in our hybrid scheme (see §IV and §V).

III. TEMPORAL COUPLING

In general there are three times involved in the coupling scheme: the MD time-step Δt_P , the time-step for the C-solver $\Delta t_C (>> \Delta t_P)$ and the averaging time Δt_{av} , which are presented below as outline two possible strategies for merging the time-evolution of C and P. The information transfer (from C→P and P→C) is updated over each time interval, Δt_C . As stated above, the P→C coupling consists firstly of a coarse-graining procedure. In particular, for any particulate quantity, Φ_i , the spatial average over each P→C cell of volume V_{PC} ($= A\Delta X_{PC}$, in figure 1) is defined as $\Phi(\mathbf{R}, t) = \sum_{i \in V_{PC}} \Phi_i / N_{PC}$, where \mathbf{R} is the position of the cell in the coarse-grained coordinates and N_{PC} is the number of particles inside V_{PC} . The time average also needs to be local with respect to the coarse-grained dynamics. To that end, the microscopic quantities are sampled over a time interval Δt_{av} which is treated as an independent parameter of the simulation:

$$\langle \Phi \rangle (R, t_C) = \frac{1}{\Delta t_C} \int_{t_C - \Delta t_{av}}^{t_C} \Phi(\mathbf{R}, t) dt. \quad (1)$$

The magnitudes Δt_C and Δt_{av} are constrained by several physical and numerical prerequisites quoted in Table 1.

There are essentially two ways to deal with the coupling of time within the hybrid scheme: sequential coupling or synchronized coupling. The diagrams in fig. 2 illustrate two possible choices for these time-coupling strategies starting from given initial conditions. In the *sequential coupling* scheme, both P and C are first moved to $t = \Delta t_C$ using the initial conditions. The C→P coupling is performed first at $t = \Delta t_C$ and the P system is advanced to $t = 2\Delta t_C \sim 300\Delta t_P$. The averaged P-information collected over time interval $\Delta t_{av} = 2\Delta t_C$ within the P→C cell is then transferred to the C domain, giving the required boundary condition to advance C towards the same time $t = 2\Delta t_C$. This procedure is suited for serial processing. More refined versions of sequential coupling can be constructed to perform averaging over times Δt_{av} greater than Δt_C .

In the *synchronized coupling* scheme both domains advance in time independently until a certain instant at which both C→P and P→C information transfers are exchanged. This scheme is suitable for parallel processing because the P and C domains are being solved concurrently. We note that in this case the averaged information from P transferred

Physical condition	Algebraic constraints	Eq.
Local Equilibrium	$\Delta t_C > \tau_{col} = 0.14\rho^{-1}T^{-1/2}$ $\Delta x > \lambda = 0.2\rho^{-1}$	C.1
Flow resolution	$\Delta t_{av} < O(0.1) \tau_{flow}$ $ \Phi^{-1} d\Phi/dx \Delta x < 1$	C.2
Accuracy	$V_{PC} \Delta t_{av} > T/(\gamma^2 \eta)$	C.3
Courant condition	$\Delta t_C < \Delta x/(2u_{flow})$	C.4

TABLE I: Constrains on the coarse grained time and length scales within our hybrid MD-CFD scheme. Condition C.1 ensures the local thermodynamical equilibrium at the averaging region: the coarse-graining time Δt_{av} and grid-spacing Δx needs to be larger than the collision time τ_{col} and the mean free path λ , respectively. In C.1 τ_{col} and λ are estimated by the hard-sphere approximation. Condition C.2 is needed to resolve the fastest flow characteristic time τ_{flow} and the spatial variation of any physical variable Φ over the control cell $|\Phi^{-1} d\Phi/dx| \Delta x$. Depending on the flow behaviour, in C.2, τ_{flow} may stand for the period of the oscillatory flow f^{-1} or for the diffusive time L_x^2/ν , etc. The accuracy condition in eq.(C.3) ensures that the signal-to-noise ratio of the transversal momentum flux in a flow with shear rate γ is greater than one (similar kind of relationships can be derived for the longitudinal momentum and energy fluxes). The conditions C.1, C.2 and C.3 are applied within the P→C cell. The last condition, C.4, ensures the stability of the numerical (explicit) scheme used for time-integration of the C flow. The characteristic velocity of the flow (on one grid space) is denoted by u_{flow} .

at any of these times is obtained during the *previous* time interval Δt_{av} . This fact introduces a delay of $O(\Delta t_{av}/2)$ in the C flow. Hence, it is important to ensure that Δt_{av} is about $O(10^{-1})$ times smaller than the fastest physical time of the flow process (see Table 1).

IV. CONTINUUM-TO-PARTICLE COUPLING AND ITS VALIDATION

The generalized forces arising from fluxes of mass, momentum and energy measured from the C flow are to be injected into the particle system at the C→P cell. Table 2 summarizes how each flux contribution arising within C is translated into the P domain.

Mass continuity is ensured by inserting or extracting particles at a rate given by eq. (T.1) in Table 2. The convection of momentum is determined by the product of the rate of particle insertion s and the average velocity of the incoming/outgoing particles $\langle \mathbf{v}' \rangle$. By injecting eq. (T.1) into eq. (T.2) it is easily seen that convection balance requires $\langle \mathbf{v}' \rangle = \mathbf{u}$. New particles are therefore introduced with velocities sampled from a Maxwellian distribution at temperature T and mean velocity \mathbf{u} . On the other hand, the local equilibrium $\langle \bar{\mathbf{v}} \rangle = \mathbf{u}$ ensures that the average velocity of any extracted particles is equal to that of the continuum prescription

Viscous and pressure forces are introduced via external forces acting on the particles at P→C. An important issue is to decide how to distribute the overall force in eq. (T.3), $\sum^{N_{PC}} \mathbf{F}_i^{(ext)}$, over the individual particles. We refer to Flekkøy *et al.* (2000) and Delgado-Buscalioni & Coveney (2003b) for a full discussion. Although in general the force to be felt by each particle i within the P→C cell can be distributed according to the particle positions (see Flekkøy *et al.* 2000), we have adopted a flat distribution $F_i^{ext} = A \Pi \cdot \mathbf{n} / N_{PC}$ because it provides by construction, a correct rate of energy dissipation in eq. (T.5) (see Delgado-Buscalioni & Coveney 2003b). Using eq. (T.1) it is seen that the balance of advected energy in eq. (T.4) implies $\langle \epsilon' \rangle = e$. The energy of each particle is composed of kinetic and potential parts, $\epsilon_i = v_i^2/2 + \psi_i(\{\mathbf{r}\}^N)$. The specific energy of the continuum is $e = u^2/2 + 3kT/(2m) + \phi$ (here ϕ is the excess potential energy). The balance of kinetic energy $\langle (v')^2 \rangle = u^2/2 + 3kT/(2m)$ is ensured by inserting the new particles with the proper Maxwellian distribution. The balance of the potential energy requires a more difficult condition $\langle \psi(\{\mathbf{r}\}^N) \rangle = \phi$ to be satisfied. When inserting a new particle, this involves finding a precise location within the C→P cell with the desired potential energy. To solve this problem in a fast and effective way we have constructed an algorithm for particle insertion called USHER (Delgado-Buscalioni & Coveney 2003c). In order to find the site with the desired energy within the complex potential energy landscape, the USHER algorithm uses a variation of the steepest descent algorithm including an adaptable displacement. For densities within the range $\rho = [0.4 - 0.8]$, the USHER scheme needs around 8–30 iterations, each one involving the evaluation of a single-force. The USHER algorithm can be also applied in other problems involving particle insertion, such as grand-canonical molecular dynamics.

Finally, eq. (T.6) in Table 2 determines the rate of heat transfer into P by conduction. This energy can be injected by reproducing a non-isothermal environment within the C→P cell. To that end we have implemented a set of (typically 2-3) Nosé-Hoover thermostats (NHT) separated by a distance d with temperatures differing by $\Delta T = [\nabla T \cdot \mathbf{n}] d$, where ∇T is the C-temperature gradient at C→P.

The decay of transversal and longitudinal waves is an excellent test for the validity of our proposed the C→P coupling as they comprise the whole set of hydrodynamic modes: shear, sound and heat waves. For these tests we implemented a set-up consisting of a P region of length L_x (with periodic boundary conditions in y and z directions)

Conserved quantity	Fluxes	P	←	C	eq.
Mass		ms	$=$	$A\rho\mathbf{u} \cdot \mathbf{n}$	(T.1)
Momentum	Convection	$ms\langle\mathbf{v}'\rangle$	$=$	$A\rho\mathbf{u}\mathbf{u} \cdot \mathbf{n}$	(T.2)
	Stress	$\langle\sum^{N_{CP}}\mathbf{F}_i^{ext}\rangle$	$=$	$A\Pi \cdot \mathbf{n}$	(T.3)
Energy	Advection	$ms\langle\epsilon'\rangle$	$=$	$A\rho\mathbf{u}\epsilon \cdot \mathbf{n}$	(T.4)
	Dissipation	$\langle\sum^{N_{CP}}\mathbf{F}_i^{ext} \cdot \mathbf{v}_i\rangle$	$=$	$A\Pi \cdot \mathbf{u} \cdot \mathbf{n}$	(T.5)
	Conduction	$\langle\mathbf{J}_Q^{ext}\rangle \cdot \mathbf{n}$	$=$	$A\mathbf{q} \cdot \mathbf{n}$	(T.6)

TABLE II: The balance of mass, momentum and energy fluxes at each $C \rightarrow P$ cell. The fluxes measured within C (third column) are imposed into P via the expressions given at the second column. The cell's surface is A , and the surface vector \mathbf{n} points outwards (fig. 1). The mass rate is $s(t)$ ($s>0$ for inserted and $s<0$ for removed particles). The velocity and energy of the inserted/removed particles are \mathbf{v}' and ϵ' respectively. The external force and heat flux inserted within the $C \rightarrow P$ cell are $\sum^{N_{PC}}\mathbf{F}_i^{ext}$ and $\langle\mathbf{J}_Q^{ext}\rangle$, respectively.

surrounded by two C domains. We initially imposed on the P system a sinusoidal (x- or y-) velocity profile along the x direction. By extracting the initial amplitudes of the spatial Fourier components of all the hydrodynamic quantities it is then possible to trace the entire time-evolution of the relaxing flow using linear hydrodynamics. In particular, this permits us to calculate at any time the generalized forces to be inserted within the $C \rightarrow P$ cell. The time evolution of the spatial Fourier components of the P-variables is finally compared with the analytical expressions. Such kinds of comparisons are shown in figures 3 and 4, for the case of a relaxing shear wave and a longitudinal wave, respectively. The excellent agreement obtained indicates that the $C \rightarrow P$ coupling protocol can be used for capturing fast and low-amplitude flows, such as those governed by sound, shear or heat waves.

The entropy perturbation, shown in fig. 5, was calculated from the temperature and density perturbative field. The results clearly show that using only one thermostat per $C \rightarrow P$ cell (denoted by 1-NHT $_{CP}$, in figs. 3 and 4) leads to negative entropy production. The pure exponential decay of heat due to diffusion is only recovered when the correct (averaged) heat flux is connected to each $C \rightarrow P$ cell; in figs. 4 and 5 we present a result with two thermostats per cell (2-NHT $_{CP}$). This result confirms that the coupling-through-fluxes scheme is the correct matching procedure.

V. PARTICLE-TO-CONTINUUM COUPLING: FINITE VOLUMES AND FLUCTUATIONS

Within the $P \rightarrow C$ cells the information coming from the particle dynamics is coarse-grained to provide boundary conditions at the “upper” C-level. In §II we introduced the averages needed to produce such information. At the $P \rightarrow C$ interface the C region receives the averaged particle-fluxes as open-flux (von Neumann) boundary conditions. The averaged mass, momentum and energy particle-fluxes through the $P \rightarrow C$ interface are constructed as follows,

$$\rho\mathbf{u} \cdot \mathbf{n}_{PC} = \frac{1}{V_{PC}} \left\langle \sum_{i=1}^{N_{PC}} m\mathbf{v}_i \right\rangle \cdot \mathbf{n}_{PC} \quad (2)$$

$$\Pi \cdot \mathbf{n}_{PC} = \frac{1}{V_{PC}} \left\langle \left(\sum_{i=1}^{N_{PC}} m\mathbf{v}_i\mathbf{v}_i - \frac{1}{2}\sum_{i,j}^{N_{PC}} \mathbf{r}_{ij}\mathbf{F}_{ij} \right) \right\rangle \cdot \mathbf{n}_{PC} \quad (3)$$

$$\mathbf{q} \cdot \mathbf{n}_{PC} = \frac{1}{V_{PC}} \left\langle \left(\sum_{i=1}^{N_{PC}} \epsilon_i\mathbf{v}_i - \frac{1}{2}\sum_{i,j}^{N_{PC}} \mathbf{r}_{ij}\mathbf{v}_i\mathbf{F}_{ij} \right) \right\rangle \cdot \mathbf{n}_{PC} \quad (4)$$

where N_{PC} is the number of particles inside the $P \rightarrow C$ cell of volume V_{PC} and \mathbf{n}_{PC} is the surface vector shown in fig. 1.

A. Hybrid finite volume: boundary conditions

Let us now illustrate how these fluxes can be injected into the C domain in the framework of the finite volumes method (Patankar 1980). The finite volumes method is ideally suited to our scheme because it exactly balances the fluxes across the computational cells. Its principle is simple. Briefly, the computational domain (C) is divided into

cells of volume V_l whose size and location is given by the nodes of a specified mesh, $\{\mathbf{R}_l\}$, $l = \{1, \dots, M_c\}$. Integrating the conservation equation $\partial\Phi/\partial t = -\nabla \cdot \mathbf{J}_\Phi$ over each computational cell (say the cell H in fig. 1) one obtains,

$$\frac{d\rho_H\Phi_H}{dt} = \frac{1}{V_H} \sum_f A_f \mathbf{J}_{\Phi,f} \cdot \mathbf{n}_f. \quad (5)$$

where A_f stands for the area of the face f and \mathbf{n}_f is the outwards normal surface vector. The volume integral of the transient term of the conservation equation has been approximated by V_H times the explicit time derivative of the value of the integrand at the cell centre, halfway between the surfaces: $\rho_H\Phi_H$. Equation (5) yields a set of ordinary differential equations (ODE's) involving the flow variables at each cell face, f . The set of equations is closed for the flow variables at the cell centre by expressing the fluxes at the interfaces $\mathbf{J}_{\Phi,f}$ in terms of differences of flow variables at neighbouring cell centres, via the constitutive relations.

Let us consider the momentum flux balance for the low Reynolds number flow of an incompressible and isothermal fluid driven by diffusion of y -velocity along x direction: $\mathbf{u} = u(x)\mathbf{j}$. In this case $\mathbf{J} \cdot \mathbf{n} = P\mathbf{i} - \eta(du/dx)\mathbf{j}$, where the surface vector of the P→C surface is $\mathbf{n} = \mathbf{i}$. Let us consider an isobaric environment and restrict ourselves to the transfer of transversal (y) momentum, governed by the momentum flux $J \equiv \mathbf{J} \cdot \mathbf{j} = -\eta\gamma$ and the shear rate $\gamma \equiv du/dx$. Integrating along the cell H (see fig. 1), using a first order space discretisation of the stress (e.g. $J_w = -\eta(u_H - u_W)/\Delta x$) and an explicit time integration scheme, one obtains

$$u_H^n = u_H(1 - 2r) + ru_E + ru_W, \quad (6)$$

where the subscripts H denote the set of cell centres $H = \{1, M\}$, and the symbols E (east) and W (west) denote variables measured: $x = E(= H + 1)$ and $x = W(= H - 1)$. The time instant is denoted by $u_H = u(x_H, t)$ and $u_H^n = u(x_H, t + \Delta t_C)$ and $r \equiv \nu\Delta t/(\Delta x^2)$, with $\nu = \eta/\rho$ the kinematic viscosity. In order to guarantee the numerical stability of the explicit scheme in eq. (6), the size of the (smallest) control cell inside the C region Δx and the time step Δt are related through $r \leq 1/2$, which corresponds to the grid-diffusive-velocity $u_{flow} = \nu/\Delta x$ in the Courant condition C.4 of Table 1. In solving eq. (6) we used a uniform grid with a typical value of $\Delta x \sim 0.5$.

In order to impose the boundary condition one needs to determine the velocity within the outer cells: at the rightmost $x = x_{M+1} = L_x$ and at the leftmost boundary (inside the P→C cell, see fig. 1) $x = x_0 = l_C - \Delta x/2$. At $x_{M+1} = L_x$ there is a rigid wall which moves at a velocity $u_{wall}(t)$ and provides the Dirichlet boundary condition $u_{M+1} = u_{wall}(t)$. The hybrid formulation is applied at the left boundary $x_0 = l_C - \Delta x/2$. To evaluate the outer velocity $u_W = u_0$ we impose the balance of momentum flux across the w surface at $x = l_C$. This means that the continuum flux evaluated at $x = w$ is made equal to the corresponding averaged particle flux $\langle j \rangle_w = -\eta(\bar{u}_H - u_W)/\Delta x$. The outer velocity to be inserted in eq. (6) is then $u_W = \bar{u}_H + \langle j \rangle_w \Delta x / \eta$. The velocity \bar{u}_H is evaluated as a linear combination of the continuum $u_H(= u_1)$ and the average particle velocity $\langle v \rangle_H$ at $x_1 = l_C + \Delta x/2$:

$$\bar{u}_H = (1 - \alpha)u_H + \alpha\langle v \rangle_H. \quad (7)$$

By inserting eq. (7) into eq. (6) one obtains the velocity at the boundary cell

$$u_H^n = u_H(1 - r) + ru_E + \frac{\langle j \rangle_w \Delta t}{\rho \Delta x_H} + \alpha r (\langle v \rangle_H - u_H). \quad (8)$$

The reason for the choice of \bar{u}_H in eq. (7) now becomes clear. It introduces the last term on the right hand side of eq. (8) which acts as a forcing term ensuring velocity continuity by gently driving the continuum velocity to the corresponding particle average $u_H = \langle v \rangle_H$. The strength of the *velocity coupling* is maximal when $\alpha = 1$ and is absent if $\alpha = 0$. The idea of using a hybrid gradient (arising for any $\alpha \neq 0$ in eq. (7)) arose from the outcome of calculations performed at very low shear rates ($\gamma < 10^{-2}$). Using $\alpha = 0$ one obtains a velocity discontinuity at P→C which is of the same order of magnitude as the fluctuations of the mean instantaneous velocity within the overlapping region. At low shear rates this means substantial relative differences in the C and P velocities, $\langle v \rangle_H - u_H / u_H \sim O(1)$. This problem is solved by introducing a small velocity coupling in the continuum scheme, with a small value of $\alpha \in [0.2, 0.5]$, which drives the continuum velocity to the average particle velocity in a time of $O[\Delta x^2/(\nu\alpha)]$. To check any influence of the velocity coupling term in eq. (8) on the flux balance, we performed simulations of the Couette flow at different shear rates and compared its average over time with the time averaged momentum particle flux. The results showed that, in average, the velocity coupling term is vanishingly small so it does not introduce any extra flux in the coarse-grained time scale.

B. The effect of fluctuations: shear stress

In our scheme, the fluctuating nature of the fluxes introduced into the C region at P→C imposes a limitation on our ability to resolve the flow field, as also arises in experiments and full MD simulations. This limit is determined by

signal-to-noise ratio becoming smaller than one. A theoretical expression for the amplitude of the stress fluctuations can be obtained (Delgado-Buscalioni *et al.* 2003), providing a relationship between the signal-to-noise ratio and the coarse-grained time and space scales Δt_{av} and V_{PC} . Table 1 contains the condition to ensure an averaged shear force larger than its variance. It is clear that in weak steady flows it is always possible to increase the signal-to-noise ratio by enlarging Δt_{av} . Nevertheless, in a general space and time-dependent flow, the sizes of the averaging windows in space and time (V_{PC} and Δt_{av}) are bounded above by the minimum wavelength and characteristic time which need to be treated within the flow. Such requirements on spatial and temporal flow resolution are also quoted in Table 1.

VI. OSCILLATORY WALL FLOW

In order to test the applicability of the full hybrid scheme under unsteady flows, we have considered the flow of an incompressible and isothermal fluid between two parallel walls in relative oscillatory motion. This set-up is widely used to investigate the rheological properties of complex fluids attached to surfaces, as polymer brushes (see C.M. Wijmans & B. Smit (2002) for a recent review). These systems are good examples of the sort of applications of the hybrid scheme, which can treat the complex fluid region by MD and the momentum transfer from the bulk by CFD. A similar set-up can be also used in the simulation of nanotechnological process. For instance, Stroock *et al.* (2002) showed that the mixing of solutions in low Reynolds number flows in microchannels can be enhanced by introducing bas-relief nano-structures on the floor of the slot. In our test flow, the simulation domain is $0 \leq x \leq L_x$ and it is periodic along y and z directions. The particle domain occupies the region $x < l_P$, and it includes the LJ liquid and the atomistic wall composed of two layers LJ particles at $x \leq 0$. The continuum domain comprises the region $x \in [l_C, L_x]$. The sizes of the simulation domains were within the nanoscale $L_x \sim 50\sigma$, and $l_P \sim 15\sigma$, while the width of the overlapping region, $l_P - l_C$, was set to around 5σ . The flow is uniquely driven by the oscillatory motion of the $x = L_x$ wall along the y direction, meaning that the mean pressure is constant throughout the domain and there are no transfers of mean energy or mass in the x direction (perpendicular to the P→C surface). Therefore the mean flow carries transversal momentum by diffusion only, and the equation of motion for the y -velocity is $\partial u / \partial t = \nu \partial^2 u / \partial x^2$, with boundary conditions $u(0, t) = 0$ and $u(L, t) = u_{wall}(t) = u_{max} \sin(\omega t)$. This equation can be solved analytically (H. Schliting 1958; C.M. Wijmans & B. Smit 2002). The flow profile has a maximum amplitude at the moving wall and the momentum introduced by its motion penetrates into a fluid layer of width $\delta \sim \sqrt{\pi \nu / f}$. Beyond this layer the flow amplitude tends to zero diffusively as it approaches the other wall held at rest. Therefore, the maximum shear rate attained inside the momentum layer is of order $\gamma \sim u_{max} / \delta$. Inserting this relation into the signal-to-noise condition (C.3 in Table 1), we find

$$\rho u_{max}^2 \Delta t_{av} > \pi f^{-1} \left(\frac{k_B T}{V_{PC}} \right). \quad (9)$$

Equation (9) means that in order to attain a signal-to-noise ratio larger than one, the mean kinetic energy per unit volume of the flow integrated over the averaging time Δt_{av} needs to be larger than the corresponding energy due to fluctuations over the period of the mean flow. It is important to mention that at low enough frequencies ($f > \nu / L^2$), there is sufficient time for momentum to be spread by diffusion over the whole domain. In such situations the correct condition is given by the signal-to-noise condition (C.3 in Table 1) with $\gamma \sim u_{max} / L^2$.

As indicated by condition C.2 in Table 1, in order to solve for the temporal variation of the flow it is required that $\Delta t_{av} f \geq O(0.1)$. Inserting this condition into eq. (9) one obtains $u_{max} > 5 \left(\frac{k_B T}{\rho V_{PC}} \right)^{1/2}$. For $k_B T = 1.0$, $\rho = 0.8$ and $V_{PC} = O(100)$ the above inequality yields $u_{max} > 0.5$. We performed oscillatory shear simulations for values of u_{max} above, close to and below the threshold given by eq. (9). As shown in fig. 6a, calculations made at large flow amplitudes are in excellent agreement with the analytical solution. In figure 6b we present results for the same density and temperature ($\rho = 0.8$ and $T = 1$) and a wall velocity $u_{max} = 0.5$ right at the accuracy limit predicted by (9). The averaging time was chosen to be $\Delta t_{av} = 10$. As shown by the instantaneous velocity within the P→C cell, the noise amplitude is nearly equal to the flow amplitude and its time-averaged value shows traces of fluctuations. Figure 6c corresponds to the same velocity and density but at a larger temperature $T = 4$. This case is below the accuracy limit (given by C.3 in Table 1) where forces arising from thermal fluctuations dominate the hydrodynamic ones.

VII. CONCLUSIONS AND FUTURE DIRECTIONS

We have presented a hybrid continuum-particle scheme for moderate-to-large fluid densities which takes into account mass, momentum and energy exchange between a domain described by discrete particle Newtonian molecular dynamics

(P) and an interfacing domain described by continuum fluid dynamics (C). The coupling scheme is applied within an overlapping region comprised of two sub-cells where the two-way exchange of information is performed: C→P and P→C. We have shown that the coupling-through-variables scheme (which simply ensures continuity of variables within the overlapping region) is not sufficient to guarantee positive entropy production. However, by generalizing the coupling-through-fluxes scheme proposed by Flekkøy *et al.*, 2000 to energy and mass transfer we find that the correct decay of shear, sound and heat waves is obtained.

We are now deploying the present scheme to study the dynamics of a tethered polymer under shear flow. The polymer and its local environment are treated via MD, while the shear flow imposed on the outer domain is treated via the finite volume CFD method. In the future, we plan to apply our hybrid scheme to the study of membrane dynamics.

Enhancements to the present hybrid algorithm are under investigation. In the scheme described here the energy flux balance is ensured only over time averages. We are currently studying alternative schemes which *exactly* balance this flux. From a numerical standpoint, we plan to implement the P→C coupling in conjunction with a finite volume CFD solver in 3D.

Also, the present scheme can be easily adapted to couple molecular dynamics with another mesoscopic scheme that takes into account hydrodynamic fluctuations. This sort of hybrid scheme could be used in applications where the fluctuations are relevant (microfluidics, fluids near critical point, etc...). An important condition for the interfacing mesoscopic scheme is that it needs to be fully consistent with thermodynamics. Also important is that the transport coefficients of the mesoscopic model should be adjustable to represent the correct coarse-grained dynamics of the selected working fluid. Natural candidates are the Lagrangian schemes involving Voronoi tessellation (Flekkøy *et al.* 2000a) or the Smooth Particle Dynamics model and related mesoscopic techniques (Español 2003). The lattice Boltzmann (LB) method is another possible candidate to interface with the MD domain. This model has been already used in multiscale modelling (Succi *et al.* 2001). Nevertheless, the problem with LB methods at present is that there is no truly reliable thermohydrodynamic model other than for single phase flow. Energy conservation remains unsolved and most models are athermal; even the thermohydrodynamic lattice-BGK models for the ideal gas are vastly over-determined and get the temperature dependence of the viscosity wrong (Boghossian and Coveney 1998). Therefore the hybrid scheme proposed here could only be interfaced with the lattice Boltzmann model in certain applications involving isothermal and incompressible single phase flows.

A longer term goal of this research is to develop a flexible, componentized, hybrid coupling environment into which *any* molecular dynamics and *any* continuum fluid dynamics codes may be inserted. This will require consideration of electrostatic forces and, therefore, an additional conserved quantity, the electric charge, whose flux coupling will require use of Poisson-Boltzmann solvers. Moreover, such multiscale hybrid schemes are attractive candidates for efficient deployment on computational grids, a feature now under investigation with the RealityGrid project (www.realitygrid.org).

VIII. ACKNOWLEDGEMENTS

We gratefully acknowledge fruitful discussions with Professor Eirik Flekkøy. This research is supported by the European Commission through a Marie Curie Fellowship to RD-B (HPMF-CT-2001-01210) and by the EPSRC RealityGrid project GR/R67699. R. D-B also acknowledges support from the project BFM2001-0290.

References

- Abraham F. F., Broughton J. Q., Berstein N. and Kaxiras E. 1998 Spanning the continuum to quantum length scales in a dynamic simulation of brittle fracture. *Europhys. Lett.*, **44** 783
- Boghossian B. and Coveney P. V 1998 Inverse Chapman-Enskog derivation of the thermohydrodynamic lattice-BGK model for the ideal gas, *Int. J. Mod. Phys. C* **9**, 1231-1245
- Delgado-Buscalioni & Coveney P. V. 2003a Continuum-particle hybrid coupling for mass, momentum and energy transfers in unsteady fluid flow, *Virtual Journal of NanoScale Science & Technology* **7**, Issue 16, April 21, <http://ojps.aip.org/nano>
- Delgado-Buscalioni R. & Coveney P. V. 2003b Continuum-particle hybrid coupling for mass, momentum and energy transfers in unsteady fluid flow, *Phys. Rev. E* **67**, 046704.
- Delgado-Buscalioni R. & Coveney P. V. 2003c USHER: an algorithm for particle insertion in dense fluids. *J. Chem. Phys.* **119**, 978.

- Delgado-Buscalioni R., Coveney P. V. and Flekkøy E. 2003, Oscillatory shear flow in liquids via hybrid continuum-particle scheme, submitted to *Phys. Rev. E*
- Español P. 2003 Dissipative Particle Dynamics, in Trends in *Nanoscale Mechanics: Analysis of Nanostructured Materials and Multi-Scale Modeling*, V. M. Harik and M. D. Salas editors (Kluwer 2003).
- Flekkøy E., Wagner G. and Feder J. 2000 Hybrid Model for Combined Particle and Continuum Dynamics. *Europhys. Lett.* **52**(3) 271-276.
- Flekkøy E, P.V. Coveney and G. De Fabritiis 2000a, Foundations of dissipative particle dynamics, *Phys. Rev. E* **62**, 2140
- Garcia A., Bell J., Crutchfield Y. and Alder B. 1999 Adaptive Mesh and Algorithm Refinement using Direct Simulation Monte Carlo. *J. Comp. Phys.*, **154**, 134.
- Hoheisel C. 1996, Computer Calculation, in *Transport properties of fluids: their correlation, prediction and estimation*, H. Millat, J.J. Dymond and C.A. Nieto de Castro eds., Cambridge University Press.
- Schliting H. 1958 *Grenzschicht-Theory*, Braun ed., Karlsruhe.
- Stroock A. D., S. K. W. Dertinger, A. Ajdar, I. Mezić, H. A. Stone, G. M. Whitesides 2002 Chaotic mixer for microchannels, *Science* **295**, 647.
- Patankar S. 1980, *Numerical Heat Transfer and Fluid Flow*, Hemisphere, New York.
- Succi et al 2001 Applying the lattice Boltzmann equation to multiscale fluid problems, *Computers in Sci. and Eng.* **3**, 26-37
- Wijmans C.M. & Smit B. 2002 Simulating tethered polymer layers in shear flow with dissipative particle dynamics. *Macromolecules* **35**, 7138-7148.

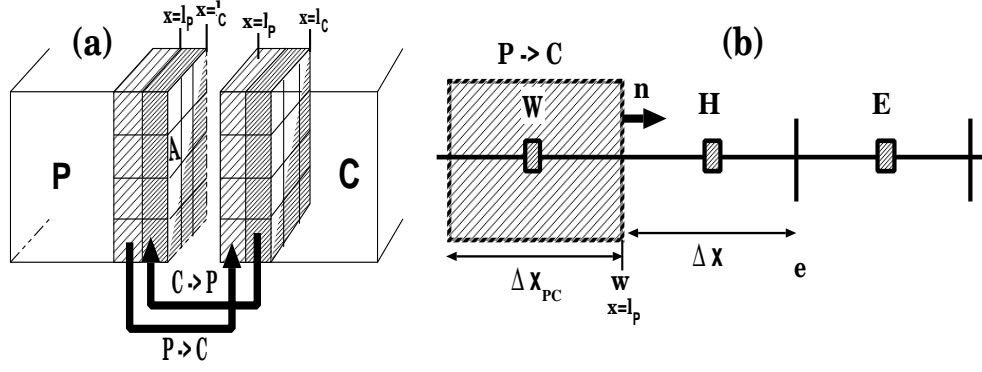


FIG. 1: The domain decomposition of the hybrid scheme: (a) displays P and C regions separatedly. The shaded region represents the overlapping domain comprised by a 2D array of C \rightarrow P and P \rightarrow C cells where the exchange of microscopic and macroscopic information is carried out. The surface area of each cell is A . (b) shows the P \rightarrow C region in more detail and the neighbouring control cells pertaining to the finite volume discretization of the C region. In this one-dimensional example, the width of the P \rightarrow C cell is Δx_{PC} and its volume is $V_{PC} = A\Delta x_{PC}$.

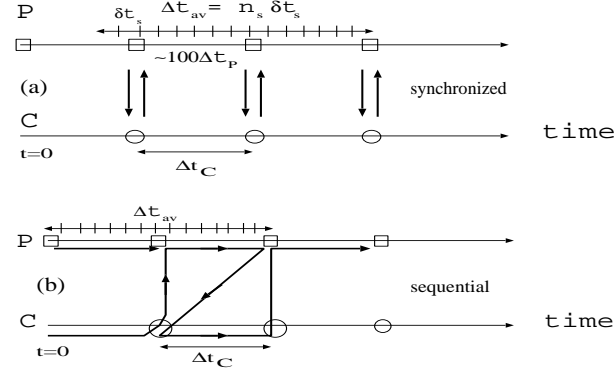


FIG. 2: Two possible time coupling strategies in a particle-continuum hybrid scheme: (a) synchronized coupling and (b) sequential coupling. Bold arrows indicate the direction of the information transfer. The time average of the P variables is performed during the time interval Δt_{av} by n_s samplings separated in time by δt_s . Δt_C and Δt_P are the continuum time step and the MD time step respectively.

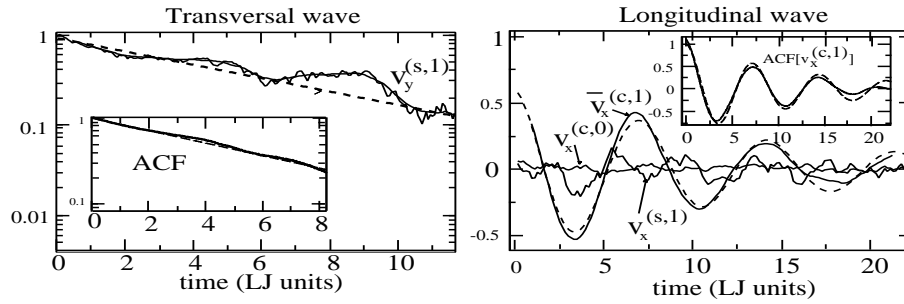


FIG. 3: The Fourier components of the transversal and longitudinal velocity perturbation. In the notation $v_y^{(s,n)}$; s indicates the sinusoidal component and c cosinusoidal and n the wavenumber $k_n = nk_0$. The transversal wave has $k_0 = 0.35$, the size of the P region was $L_x = 20$ (in LJ-units) and the temperature was $T = 2.5$; while for the longitudinal wave $k_0 = 0.168$, $L_x = 40$ and $T = 3.5$. In both cases $\rho = 0.53$. The autocorrelation of the velocity is also shown. In all graphs the dashed lines are the analytic solution from linear hydrodynamics. Reproduced from R. Delgado-Buscalioni & Coveney 2003b with permission

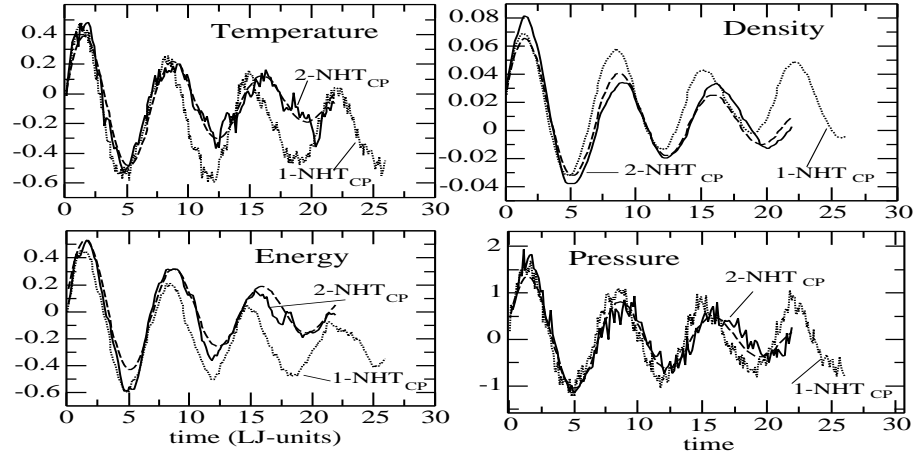


FIG. 4: The dominant Fourier mode of the various thermodynamic variables in the decay of the same longitudinal wave shown in figure 3. Comparison is made between a calculation with two Nosé-Hoover thermostats per C \rightarrow P cell (2-NHT_{CP}) and another using only one thermostat (1-NHT_{CP}). Dashed lines are the analytical hydrodynamic solution. The entropy production from these two simulations is shown in figure 5, only the one with two thermostats yields the correct physical behaviour. Reproduced from R. Delgado-Buscalioni & Coveney 2003b with permission

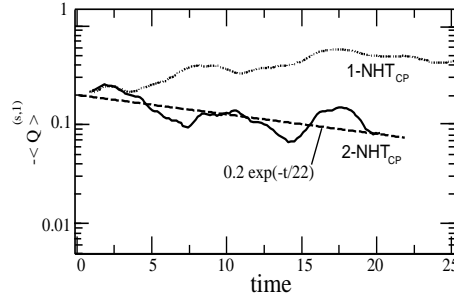


FIG. 5: The main Fourier mode of the entropy density (as a product with the mean temperature) $-\langle Q^{(s,1)} \rangle$ time-averaged along $\Delta t_{av} = 1.0$. The result comes from the same longitudinal wave shown in figs. 3 and 4. Comparison is made between a flux-coupling scheme (using 2-NHT_{CP}) and the coupling-state scheme using 1-NHT_{CP} (cf. fig. 4). The latter violates the second law of thermodynamics. The dashed line is the analytical hydrodynamic result. Reproduced from R. Delgado-Buscalioni & Coveney 2003b with permission.

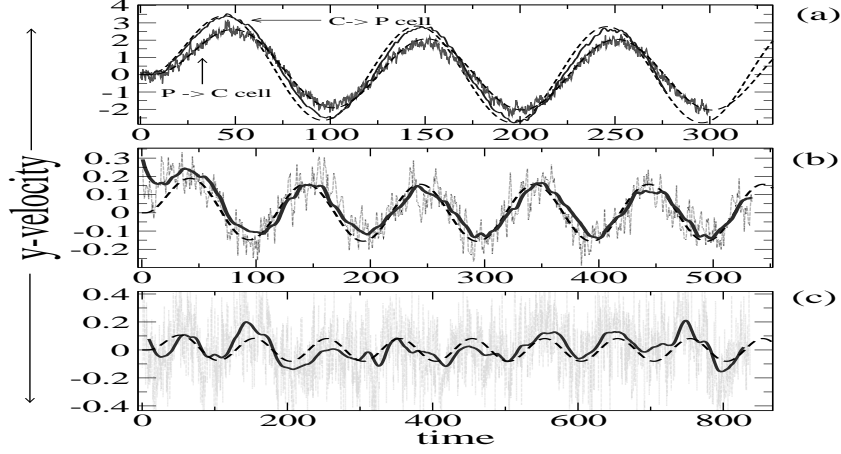


FIG. 6: Mean molecular velocities within the overlapping region for several oscillatory-wall shear flows applied to a LJ fluid; u_{\max} is the maximum wall velocity and f its frequency. (a) Flow corresponds to $u_{\max} = 10$, $f = 0.01$ and $T = 1.0$; we plot the instantaneous particle velocity at $P \rightarrow C$ and the time-averaged particle velocity (along $\Delta t_{av} = 1$) at $C \rightarrow P$; (b) corresponds to $u_{\max} = 0.5$, $f = 0.01$ and $T = 1.0$; (c) to $u_{\max} = 0.5$, $f = 0.01$ and $T = 4.0$. In all cases $\rho = 0.8$, the extent of the periodic directions are $L_y = L_z = 9$, while $V_{PC} = \Delta x L_y L_z = 178$. In (b) and (c) we show the $P \rightarrow C$ mean velocity (instantaneous and time-averaged velocity with $\Delta t_{av} = 10$); dashed lines are the analytical hydrodynamic solutions of the imposed shear flows. All quantities are given in reduced LJ units.